Plastic hardening model II: Calibration and validation

Z. Cheng & A. Lucarelli
Itasca Consulting Group, Inc., Minneapolis, MN, USA

ABSTRACT: The shear strength and other material parameters of the soil using the plastic hardening model can be determined from geotechnical test data. A calibration procedure for the plastic hardening model based on a set of triaxial lab tests on Monterey sand is demonstrated and discussed. A validation example presents a case study of tunnel excavation where the numerical simulation is compared with the measured data.

1 INTRODUCTION

The conventional Mohr-Coulomb (MC) model is widely used in civil engineering, especially for the prediction of failure phenomena such as slope engineering using the so-called strength reduction method. The MC model uses a constant stiffness for both loading and unloading. If the stiffness is adopted by the initial slope from a stress-strain lab test curve, it will underestimate the deformation before failure. If the stiffness is taken as some averaged stiffness before failure, the unloading-reloading stiffness will not be realistic, which could predict some unrealistic lifting behind the retaining wall after excavation. The plastic hardening (PH) model is based on the work of Schanz et al. (1999), which extends the hyperbolic Duncan-Chang non-linear elastic model (Duncan & Chang 1970) to an elastoplastic counterpart to provide better pre-failure stress-strain relation. Different stiffness values are introduced for primary loading and unloading/reloading in the PH model. The yield surface of the PH model is not fixed in the principal stress space, but it can expand due to the increase of the plastic strain, which is termed as plastic hardening.

We present herein a calibration procedure based on a series of lab tests; and a simulation example showing the validation of the model. The formulation and implementation in *FLAC3D* (Itasca 2012) can be found in a related paper (Cheng & Detournay 2016) and the calibration procedure based on the in-situ tests and a design application can be found in Lucarelli & Cheng 2016.

2 CALIBRATION FROM TRIAXIAL COMPRESSION TESTS

The shear strength of the soil may be determined by performing different laboratory tests such as a direct shear test, ASTM D3080, unconfined compression test, ASTM D2166, and triaxial compression test (ASTM D2850) or in-situ tests (standard penetration test, ASTM D1586, corn penetration test, ASTM D3441, van shear test, ASTM D2573 (Coduto 2015)). This section presents how most material parameters can be readily calibrated from the conventional geotechnical laboratory tests.

The calibration example uses the original test results obtained from the triaxial compression tests of Monterey sand (Lade 1972). The triaxial test consisted of loading the specimen, followed by unloading-reloading regimes. The data are based on three sets of triaxial compression tests with confining pressures of 1.2, 0.6, and 0.3 kgf/cm^2 (follow the same pressure unit as the original data). The initial void ratios are 0.783, 0.786, and 0.781, respectively.

2.1 *Calibration of friction angle ϕ and cohesion c*

The procedure is quite standard, which analyzes deviatoric stress q vs. normal stress p using triaxial compression test lab data. The procedure uses a trend line to fit the Mohr-Coulomb envelope, and the slope of the line $= 6\sin\phi\,/(3-\sin\phi)$, which determines the friction angle ϕ. The intercept of the line $= 6c\cdot\cos\phi\,/(3-\sin\phi)$, which determines cohesion c, as the friction angle ϕ, is already known. The slope of the trend line of the Mohr-Coulomb envelope presented in Figure 1 is 1.403. Based on this, the friction angle is calculated to be 34.65°. The intercept is zero, which implies that the cohesion is zero.

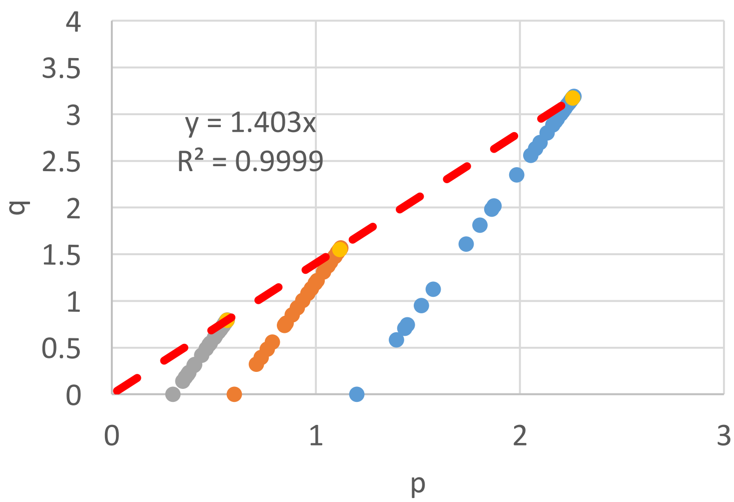

Figure 1. Determination of the friction angle and cohesion from three sets of triaxial compression tests with three different confining stresses.

2.2 *Calibration of $\boldsymbol{R_f}$, $\boldsymbol{m}$ and $\boldsymbol{E_{50}^{ref}}$*

The procedure to determine these three parameters includes plotting the curve of ε_1/q vs. ε_1/q_f using the triaxial compression test lab data and using a trend line to fit the data. The slope of the line is R_f and the intercept is $1/E_i$. Three sets of triaxial compression tests with three different confining pressures can be used to produce three pairs of R_f, E_{50}. The final R_f is the averaged one and the pairs of E_i,σ_3 will determine m and E_{50}^{ref}. Figure 2 plots the curves of ε_1 / q versus ε_1 / q_f using triaxial compression test lab data of the Monterey sand with confining pressures 1.2, 0.6, and 0.3 kgf/cm^2. The slopes of these lines are R_f, and the intercepts are $100/E_i$ (as strain is given in %). This figure determines three pairs of R_f, E_{50}, which are summarized in Table 1. The average R_f is 0.957. Parameter p^{ref} needs no calibration (its value is assumed to be 0.1 kgf/cm^2). Finally, plot parameters ln $(-\sigma_3/p^{ref})$ versus ln (E_{50}), as shown in Figure 3 (remember that cohesion $c = 0$). The slope of the trend line in Figure 2 determines $m = 0.707$ and the intercept determines $E_{50}^{ref} = \exp(4.63) = 102.5$ kgf/cm^2.

Table 1. Determination of $\boldsymbol{R_f}$, $\boldsymbol{m}$ and $\boldsymbol{E_{50}^{ref}}$.

σ_3	R_f	$1/E_i$	E_i	E_{50}	$\ln(E_{50})$	$\ln\left(\frac{c\cdot\cot\phi-\sigma_3}{c\cdot\cot\phi+p^{ref}}\right)$
-0.3	0.9558	0.002459	406.7	212.3	5.358	1.099
-0.6	0.9678	0.001286	777.6	401.3	5.995	1.792
-1.2	0.9476	0.00093	1075.3	565.8	6.338	2.485

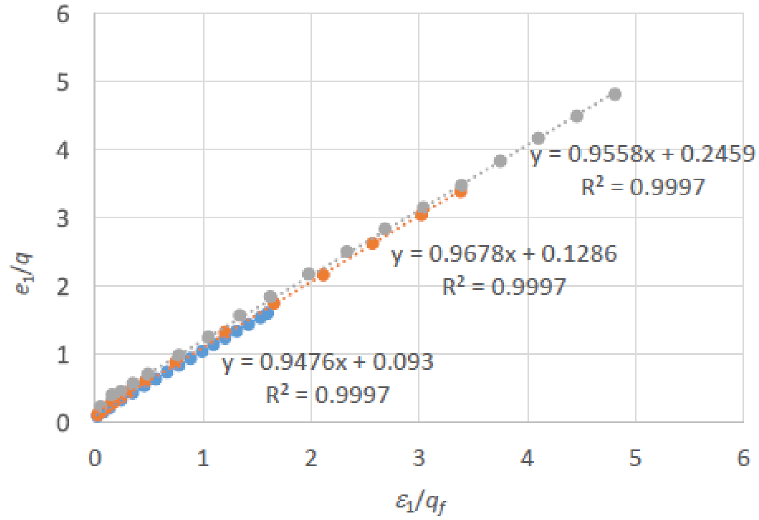

Figure 2. Determination of $\boldsymbol{R_f}$ and $\boldsymbol{E_i}$ from three sets of triaxial compression tests with three different confining stresses.

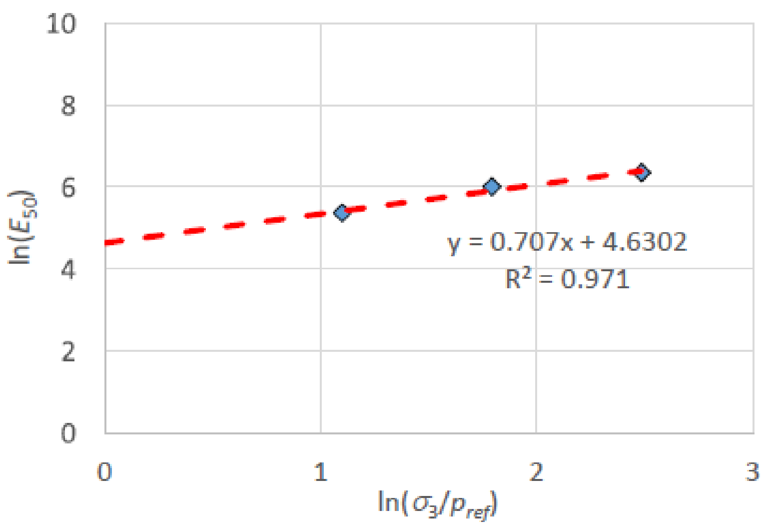

Figure 3. Determination $\boldsymbol{m}$ and $\boldsymbol{E_{50}^{ref}}$ from three sets of triaxial compression tests with three different confining stresses.

2.3 *Calibration of* $\boldsymbol{E_{ur}^{ref}}$

After the calibration of parameter m, E_{ur}^{ref} is calibrated using the unloading-reloading moduli E_{ur} obtained from the original q versus ε_1 data in the triaxial compression test. The final value of E_{ur}^{ref} can be the averaged using data for different confining pressures. For the Monterey sand example, E_{ur}^{ref} is determined to be 320 kgf/cm^2. If the unloading-reloading moduli are not available, a value in the range of $(3-5) \times E_{50}^{ref}$ can be used for most soils. The PH model uses a default value of $4 \cdot E_{50}^{ref}$ if no input is provided for E_{ur}^{ref}.

2.4 *Calibration of dilation angle* $\boldsymbol{\psi}$

The dilation angle can be calibrated from the $\varepsilon_v - \varepsilon_1$ data of the triaxial compression tests. The maximum dilation slope of the $\varepsilon_v - \varepsilon_1$ curve is approximately $2\sin\psi/(1-\sin\psi)$. For Monterey sand, the dilation angles are 6–7°. The values are summarized in Table 2.

Table 2. Calibrated material parameters for loose Monterey sand.

Material Parameters	S3 = 1.2 kgf/cm^2	S2 = 0.6 kgf/cm^2	S3 = 0.3 kgf/cm^2
E_{50}^{ref} (kgf/cm^2)		102.5	
E_{ur}^{ref} (kgf/cm^2)		320	
m		0.707	
R_f		0.957	
p^{ref} (kgf/cm^2)		0.1	
Poisson 's ratio (ν, -)		0.3	
Friction angle (ϕ, °)		34.65	
Cohesion (c, kgf/cm^2)		0.0	
Max void ratio (e_{max})		0.803	
sig1, sig2, sig3	1.2	0.6	0.3
ocr (kgf/cm^2)	1.0	2.0	4.0
Initial void ratio (e_{ini})	0.783	0.786	0.781
Dilation angle (ψ, °)	6.1	6.4	7.0
All other		default values	

2.5 *Calibration of $\boldsymbol{K_{nc}}$ and $\boldsymbol{E_{oed}^{ref}}$*

These two parameters can be calibrated from the oedometer tests. The ultimate value of σ_3/σ_1 from the oedometer test is K_{nc}. For the case of $\sigma_1 = p_{ref}$, the tangent modulus of $\sigma_1 - \varepsilon_1$ curve is E_{oed}. E_{oed}^{ref} can be determined using E_{oed} and values of m and cohesion determined previously. If the data of oedometer tests are not available, the PH model uses the default values of $K_{nc} = 1 - \sin\phi$ (Kulhawy & Mayne 1990), $E_{oed}^{ref} = E_{50}^{ref}$. For most soils, values for K_{nc} are in the range 0.5–0.7. For this example, the oedometer test data are not available, so the default values are used.

2.6 *Calibration of elastic Poisson's ratio*

Elastic Poisson's ratio can be estimated from the unloading-reloading slope of the $\varepsilon_v - \varepsilon_1$ curve. Experience shows that results are not very sensitive to changes in Poisson's ratio, and therefore Poisson's ratio in the range of 0.15 to 0.40 is typically used. In this example, Poisson's ratio is assumed to be 0.3.

2.7 *Calibration of void_max*

The material parameter of void_max is needed if the dilation smoothing technique is required. The value of void_max can be determined by conducting standard laboratory tests (ASTM D4254). If the standard ASTM D4254 laboratory test data are not available, its value can be estimated through a trial-and-error method based on the curves of the volumetric strain versus axial strain of the triaxial compression tests. In this example, its value is estimated to be 0.803. The default value is 999.0, which implies that the dilation smoothing technique will not be activated.

2.8 *Calibration of other parameters*

Such material parameters as sig1, sig2, sig3, void_ini, and *ocr* are known initial parameters (need no calibration) and should be consistent with the initial conditions.

Summary of all material properties determined for the Monterey sand is provided in Table 2. The triaxial compression tests can be reproduced by the PH model using these parameters. The results are presented in Figure 4 and Figure 5 and reveal close match between the simulated results and lab test data.

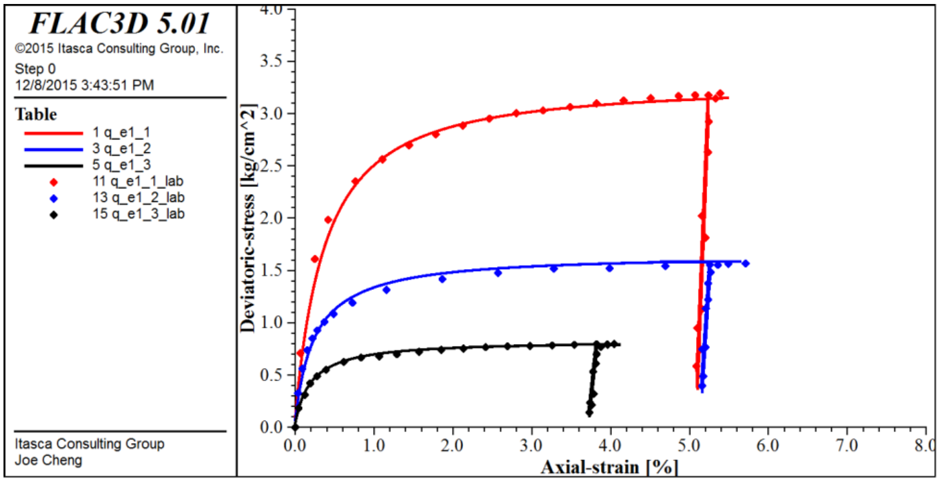

Figure 4. Deviatoric stress vs. axial strain for consolidated drained triaxial compression tests on fine Monterey sand.

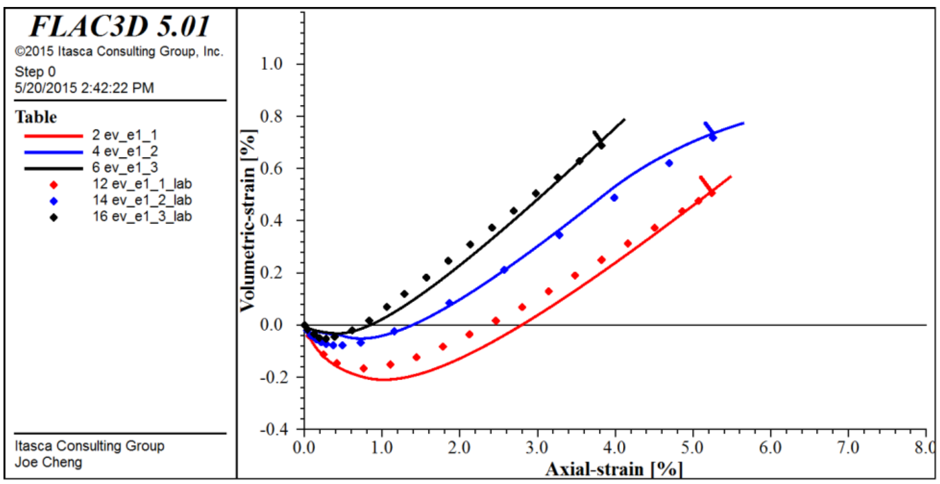

Figure 5. Volumetric strain vs. axial strain for consolidated drained triaxial compressor tests on fine Monterey sand.

3 SOUTH TOULON TUNNEL: NUMERICAL BACK-ANALYSIS

Full-face excavation with ground reinforcement has become a common technique to build large tunnels in different soil/rock conditions. Full-face excavation brings many advantages in terms of logistics and production, but it remains a difficult task to assess the performance/effectiveness of the reinforcement and support at the design phase. The face itself behaves as a temporary support for the cavity and the level of confinement provided by reinforcement elements becomes an important variable for the stability and settlement evaluation. The observational method is a crucial aspect of the design since it allows for data collection in real time and optimizing/modifying the excavation/support system. In this particular case, a monitoring section has been installed during the construction of the tunnel, which has provided good quality data for a back analysis. A *FLAC3D* model has been set-up using the plastic hardening model recently developed. All the data concerning the geology and geometry has been obtained from the papers by Janin et al. (2012 & 2013).

3.1 *Geotechnical conditions and instrumentation*

Borehole investigations show a fairly horizontal stratigraphy with a high degree of alteration of the bedrock. Figure 6 shows the local stratigraphy along with the instrumentation installed in the monitoring section. The instrumentation is composed of two inclinometers on both sides of the tunnel, one vertical extensometer on the tunnel axis and three target prisms. In addition, four radial extensometers, six vibrating wire strain gauges on the steel rib, five pressure cells, and convergence targets were installed from inside the tunnel.

3.2 *FLAC3D numerical model*

A three-dimensional model has been set up to analyze the tunnel excavation process using *FLAC3D* version 5 (Itasca 2012). The model takes advantage of the symmetry of the problem. The cross-section of the excavation has an area of about 120 m^2 and has been generated using the *FLAC3D* built-in extruder tool that can generate a 2D mesh and then extrude it to a 3D mesh. The extension of the model in the transversal direction is of 150 m in order to mitigate boundary effects. The depth of the crown of the tunnel is about 25 m. The grid has been densified (using the command densify multiple times) around the region of interest. Figure 7 shows the geometry of the model.

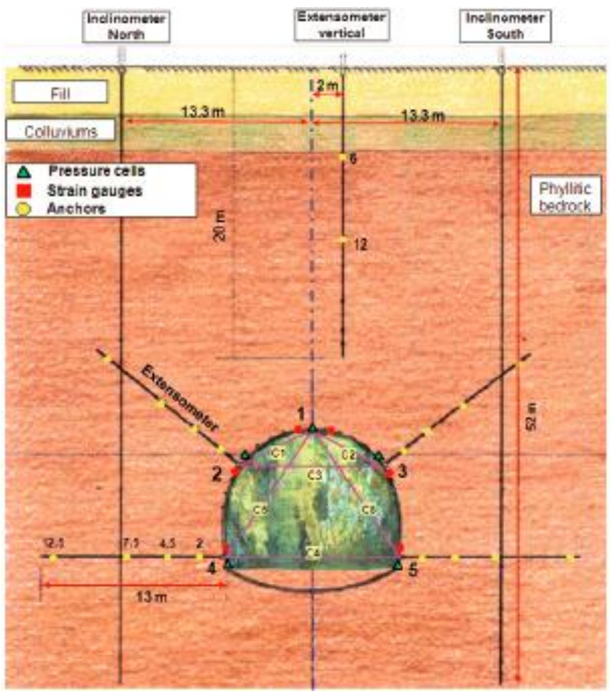

Figure 6. Stratigraphy and instrumentation (after Janin et al. 2013).

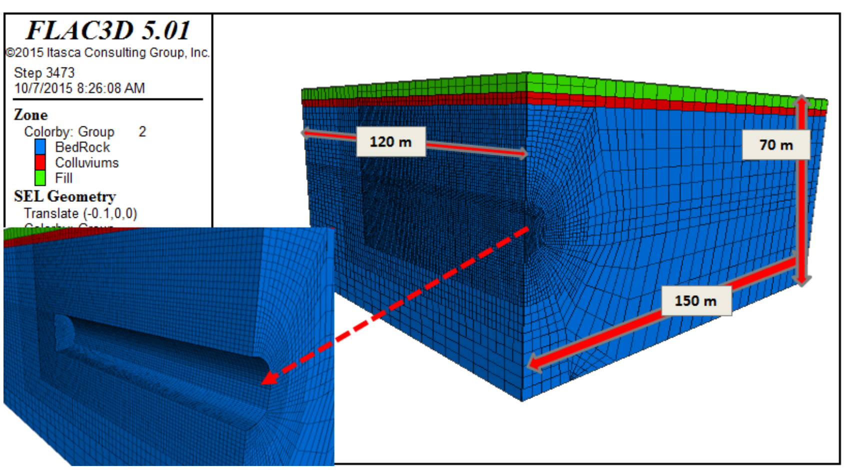

Figure 7. Geometry of the model.

3.3 *Constitutive model's parameters and simulation of the excavation process*

The soil is modeled as nonlinear elasto-plastic material using a plastic hardening model implemented in Itasca's continuum codes, *FLAC* (Itasca 2011) and *FLAC3D* (Itasca 2012). The PH model is particularly useful for excavation problems and has demonstrated that it provides a more realistic description of the problem than the Mohr-Coulomb model. Table 3 summarizes the parameters adopted. The α parameter that describes the shape of the volumetric cap is calculated internally by the program (Cheng & Detournay 2016).

Table 3. Material parameters used for numerical simulation.

Parameter	Fill	Colluvium	Bedrock	Unit
Depth	0.0 to 3.5	3.5 to 5.9	Below 5.9	[m]
γ	19.0	20.8	24.2	[kN/m^3]
$E_{50}^{ref} = E_{oed}^{ref}$	1600	40000	240000	[kPa]
$E_{ur}^{ref} = 3 \cdot E_{50}^{ref}$	4800	120000	720000	[kPa]
p_ref	100	100	100	[kPa]
m	0.5	0.5	0.5	
OCR	1.0	1.0	1.0	
c'	2	10	40	[kPa]
φ'	20	30	25	[°]
ψ	0	0	0	[°]
υ	0.2	0.2	0.2	
R_f	0.9	0.9	0.9	

3.4 *Structural elements, reinforcement and support*

The face reinforcement (fiberglass elements) and the forepoling are modeled with embedded pile elements. Figure 8 shows the geometry.

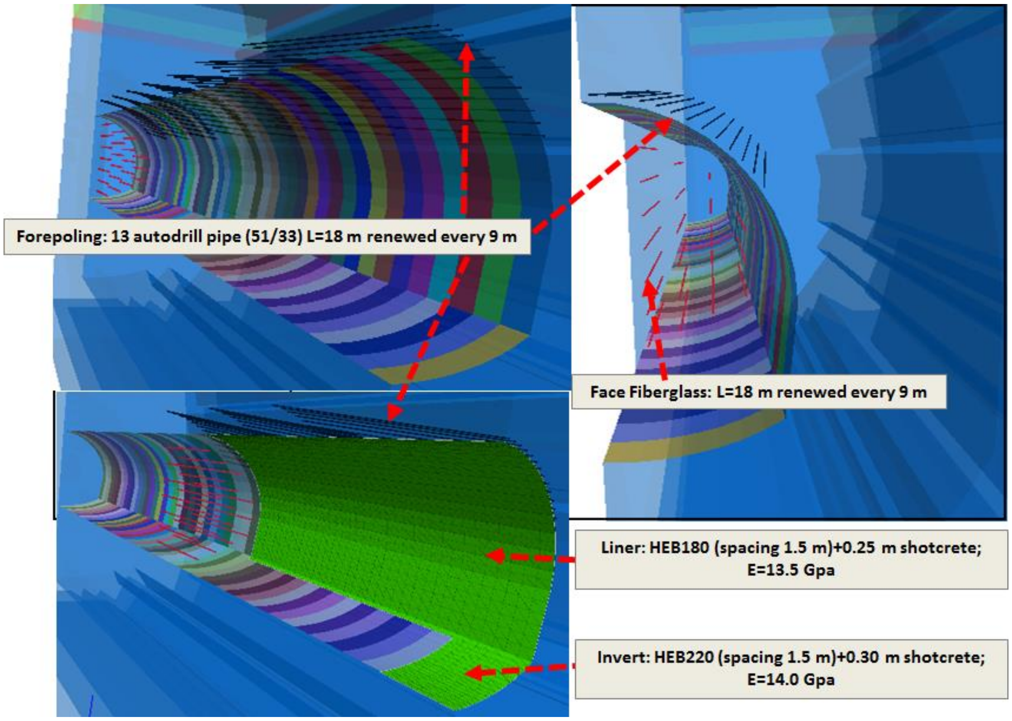

Figure 8. Structural elements layout.

3.5 *Excavation sequence*

The excavation is carried out in 1.5-m steps. Every 9 m the face reinforcement and roof forepoling are renewed. Each step is relaxed gradually before being nulled and so are the structural elements at the face. After equilibrium is reached, the liner is activated to support the free span. Figure 9 shows the excavation sequence. The whole process is managed via *FISH* and can easily be parametrized in order to test quickly different hypothesis.

3.6 *Main results*

The main results in terms of displacements are presented in Figures 10-12. The longitudinal (Fig. 10), transversal (Fig. 11) and horizontal displacement at the inclinometer (Fig. 12). The results are in good agreement with the measurements and the model is capable of capturing the main feature observed in the field. As far as the longitudinal displacement is concerned, the model seems to provide a "stiffer" response behind the face. This is mainly due to some simplification adopted to model the face reinforcement due to lack of information. Otherwise the development of the displacement as the face moves forward is captured with satisfactory agreement.

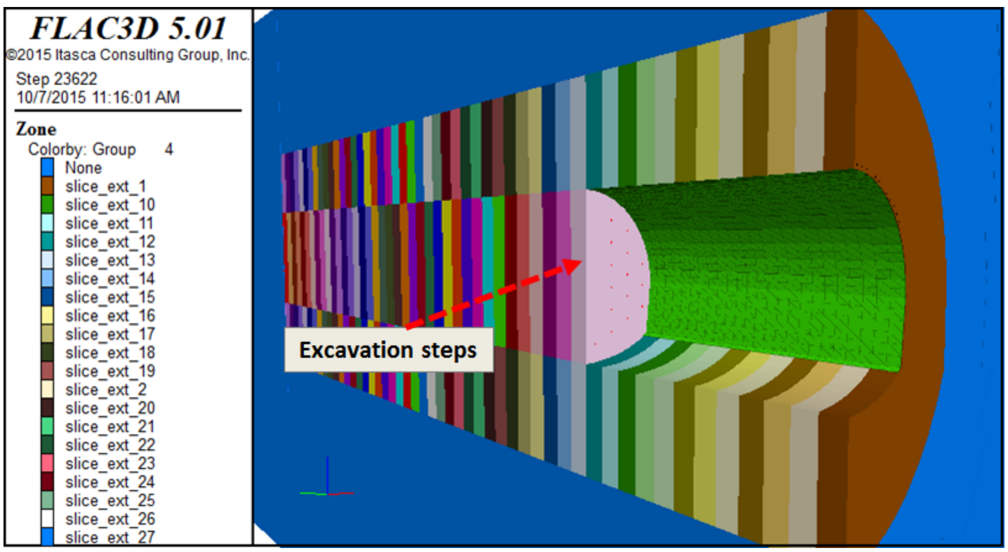

Figure 9. Excavation sequence.

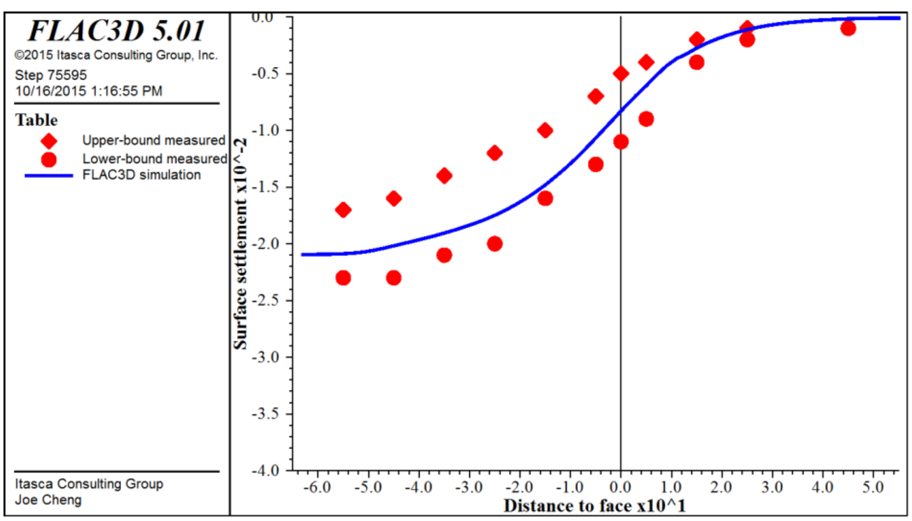

Figure 10. Vertical displacement at ground level long the tunnel axis (dots are upper- and lower-bound measured data, and the solid line is the simulated result).

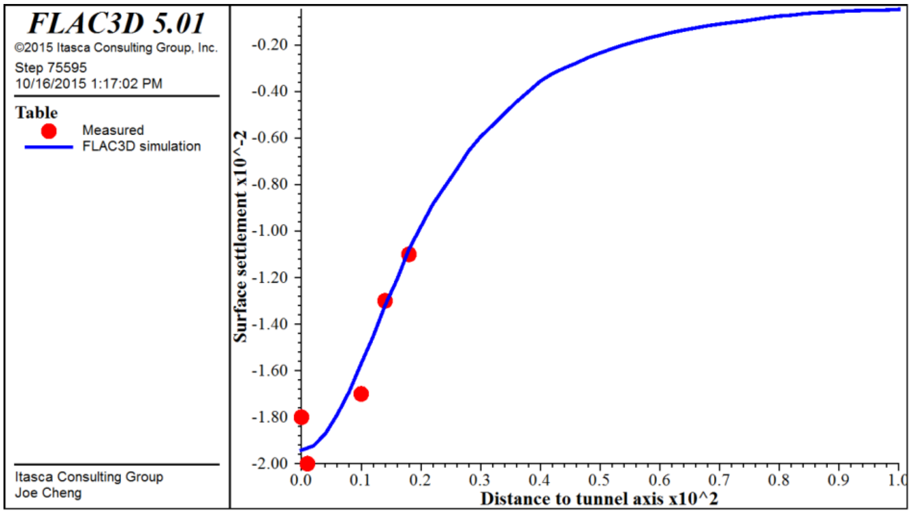

Figure 11. Vertical displacement at ground level in the transversal direction (dots are measured data, and the solid line is the simulated result).

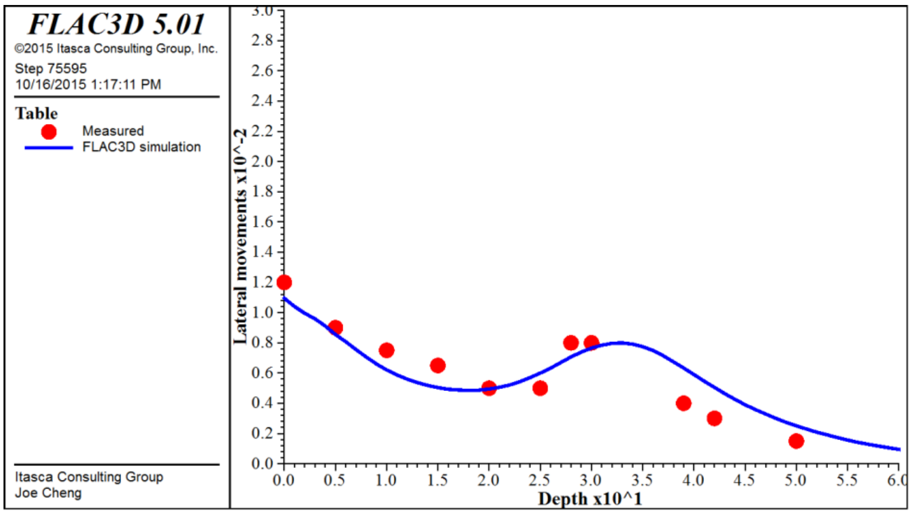

Figure 12. Horizontal displacement at the inclinometer's position (dots are measured data, and the solid line is the simulated result).

4 SUMMARY

The plastic hardening model is a flexible and user-friendly constitutive model that accommodates the most important features of the non-linear behavior of soils. It is easy and straightforward to calibrate the material parameters from the laboratory tests. This tunnel excavation case study validates the implemented model by a good match between the simulated results and the measured data.

REFERENCES

Cheng, Z. & Detournay, C. 2016. Plastic hardening model I: Implementation in *FLAC3D*. In P. Gomez, C. Detournay, R. Hart, M. Nelson (eds), *Proc. 4th Itasca Symposium on Applied Numerical Modeling. March 7-9, 2016, Lima, Peru*.

Coduto, D.P. 2015. *Foundation design: principles and practices*. Prentice Hall.

Duncan, J.M. & Chang, C.Y. 1970. Nonlinear analysis of stress and strain in soil. *J. Soil Mech. Found. Div*. 96(5), 1629-1653.

Itasca Consulting Group, Inc. 2011. *FLAC – Fast Lagrangian Analysis of Continua, Ver. 7.0*. Minneapolis: Itasa.

Itasca Consulting Group, Inc. 2012. *FLAC3D – Fast Lagrangian Analysis of Continua in 3 Dimensions, Ver. 5.0*. Minneapolis: Itasca.

Janin, J.P., Le Bissonnais H., Guilloux A., Dias D., Kastner R. & Emeriault, F. 2013. South Toulon Tube: Numerical Back-analysis of In-situ Measurements. *Plaxis Bulletin*, 33, 2013.

Janin, J.P., Dias D., Kastner R., Emeriault F., Guilloux A. & Lebissonnais, H. 2012. South Toulon tunnel: Analysis of an instrumented section. In Viggiani (ed), *Geotechnical Aspects of Underground Construction in Soft Ground*, London: Taylor & Francis Group.

Lade, P.V. 1972. *The stress-strain and strength characteristics of cohesionless soils*. Ph.D. Thesis, University of California, Berkeley, Berkeley, CA.

Lucarelli, A. & Cheng, Z. 2016. Plastic hardening model III: Design application. In P. Gomez, C. Detournay, R. Hart, M. Nelson (eds), *Proc. 4th Itasca Symposium on Applied Numerical Modeling. March 7-9, 2016, Lima, Peru*.

Kulhawy, F.H. & Mayne, P.W. 1990. Manual on estimating soil properties for foundation design. No. EPRI-EL-6800. Electric Power Research Inst., Palo Alto, CA; Cornell Univ., Ithaca, NY. Geotechnical Engineering Group.

Rowe, P.W. 1962. The stress-dilatancy relation for static equilibrium of an assembly of particles in contact. *Proc. Roy. Soc. A.* 269(1339), 500-527.

Schanz, T., Vermeer, P.A., Bonnier, P.G. 1999. The hardening soil model: formulation and verification. In R.B.J. Brinkgreve (ed), *Beyond 2000 in Computational Geotechnics -10 Years of Plaxis*. Rotterdam: Balkema.